

Experimental approach to transverse wave-number selection in cavity nonlinear optics

Adolfo Esteban-Martín,* Javier García, Eugenio Roldán, Victor B. Taranenko, and Germán J. de Valcárcel
Departament d'Òptica, Universitat de València, Dr. Moliner 50, 46100-Burjassot, Spain

Carl O. Weiss
Physikalisch-Technische Bundesanstalt, Bundesallee 100, 38116 Braunschweig, Germany
 (Received 15 December 2003; published 23 March 2004)

Spontaneous transverse pattern formation is experimentally studied in a BaTiO₃ photorefractive oscillator under degenerate four-wave mixing conditions. A near self-imaging resonator of high Fresnel number and quasi-one-dimensional in the transverse plane is used. A fine control technique of the cavity detuning, Ω , is described. It allows a precise study of the relation of Ω with the transverse wave number k_{\perp} of the roll patterns selected by the system. The law $k_{\perp}^2 = -\Omega/a$ is verified, which evidences that wave-number selection is mainly dictated by the cavity geometry. The experimentally obtained value of the diffraction parameter a matches the theoretical prediction within the error intervals. The bifurcation diagram obtained by varying Ω shows homogeneous states and domain walls for positive Ω , roll patterns for negative Ω , and nonperiodic patterns for intermediate, negative detuning values. The latter are interpreted also in the frame of the cavity selection mechanism by taking into account the finesse of the cavity.

DOI: 10.1103/PhysRevA.69.033816

PACS number(s): 42.65.Sf, 47.54.+r, 42.65.Hw

I. INTRODUCTION

Spontaneous pattern formation is common to many dissipative, nonlinear systems [1–3]. The interplay between dissipation, nonlinearity, spatial coupling, and the feed of energy into the system can provide by itself an ordering in the form of periodic patterns. These patterns are characterized by their wave number and their symmetries. Nonlinear optics offers a rich variety of systems where pattern formation takes place [4–6]. In large aspect ratio (high Fresnel number) nonlinear optical resonators, the cavity is mainly responsible for wave-number selection while the symmetries of the patterns depend on the form of the nonlinearity. The mechanism of wave-number selection in these oscillators is based on the resonance of tilted waves with respect to the cavity axis [7,8]. It is in fact a consequence of the spatial filtering brought about by the passive resonator (interferometer) which also manifests, e.g., in the off-axis, spontaneously emitted photons by an atom in a microcavity, properly detuned from the atomic resonance [9].

In the paraxial approximation, the spontaneously selected transverse wave number k_{\perp} is predicted to follow the law

$$k_{\perp}^2 = -\Omega/a, \quad (1)$$

where $\Omega = \omega_c - \omega$ is the cavity detuning parameter, ω is the frequency of the light, ω_c is the frequency of the closest cavity mode, and a is a diffraction parameter that depends on the geometry. For negative Ω , Eq. (1) can be fulfilled and tilted wave emission is predicted as $k_{\perp} \neq 0$. On the contrary for positive Ω no transverse wave number can satisfy Eq. (1) and on-axis emission is expected. This mechanism is of general validity provided that one takes into account the shift of

the cavity frequency ω_c caused by possibly existing linear and nonlinear dispersions [5].

Law (1) is found in theoretical studies of many different nonlinear optical systems [4–6]. From the experimental side some studies have reported qualitative results on the dependence of the transverse wave number on the detuning [10–13]; experimental quantitative verifications of those predictions are however almost lacking. In particular, Ackemann *et al.* [14] have demonstrated Eq. (1) in a broad-area vertical-cavity regenerative amplifier by varying the frequency of the external master oscillator (the cavity frequency was constant by construction of the device); Bortolozzo, Villoresi, and Ramazza [15] have evidenced law (1) in a nondegenerate four-wave mixing photorefractive oscillator by varying the cavity frequency. Nondegeneracy is a key feature in Ref. [15] as it allows to fix the cavity resonances by beating the signal with the pump. As a drawback, their system does not support stable patterns, and law (1) was inferred from transients.

Here we report the experimental study of Eq. (1) in a degenerate four-wave mixing photorefractive oscillator. The frequency degeneracy between pump and signal entails a phase sensitivity of the system that favors pattern stability. As a drawback, this degeneracy forbids to measure the cavity detuning by beating, as in Ref. [15], and a new technique is used, which is described. The agreement between our measurements and law (1), as theoretically evaluated, is remarkable. For negative detunings rolls are found, while for positive detunings homogeneous (on-axis) emission as well as domain walls are observed. For small and negative detunings the system shows nonperiodic stripe patterns, which are also interpreted in the frame of the commented cavity selection mechanism when the finite linewidth of the cavity is taken into account.

II. EXPERIMENTAL SETUP

The system under study is a photorefractive oscillator in a degenerate four-wave mixing configuration. Two counter-

*Email address: adolfo.esteban@uv.es

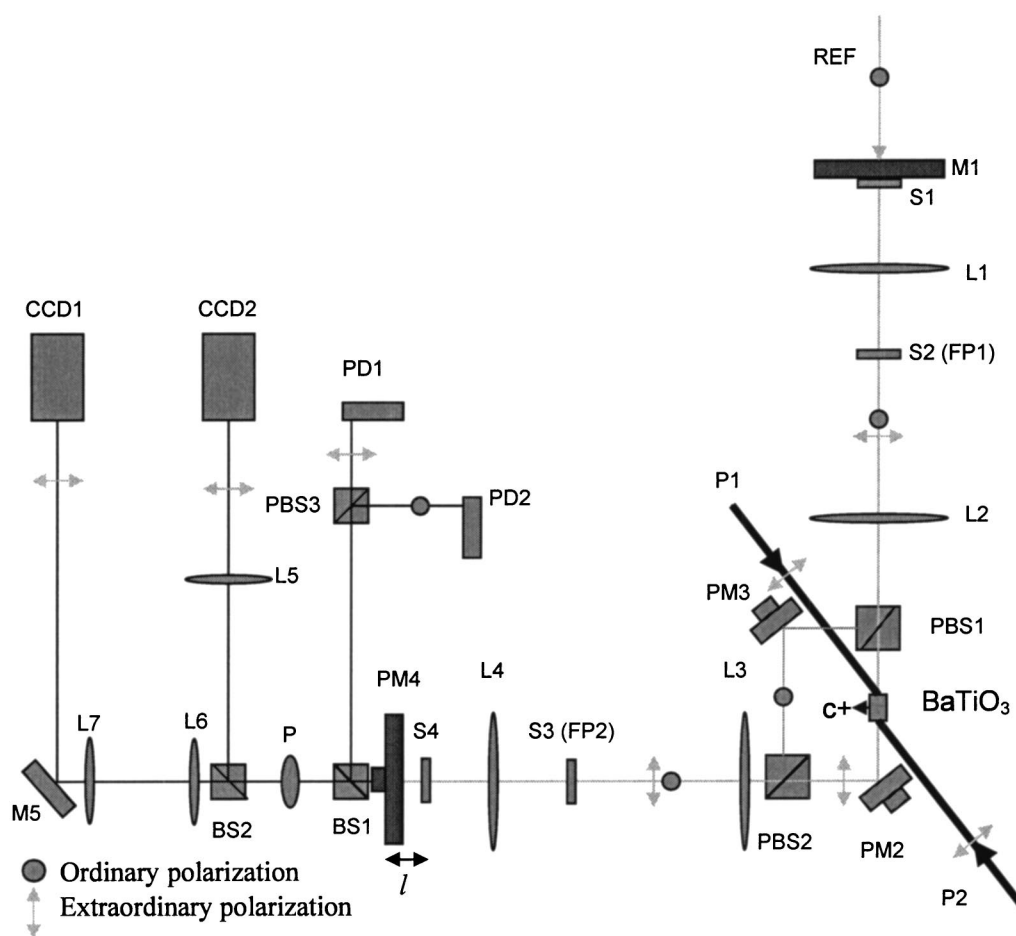


FIG. 1. Scheme of the experimental setup. See Sec. II for an explanation of the symbols.

propagating pump beams illuminate a BaTiO_3 crystal which produces scattered light, part of which seeds the oscillation in a Fabry-Perot resonator. Starting from this random seed the emission along the resonator is dynamically ruled by the gain (that gives the fraction of light that is diverted from the pumps to the resonator), the losses, the detuning, and the diffraction (defined by the resonator geometry). Each of these parameters can be, to a certain extent, controlled experimentally. The gain can be modified by the relative orientation among the crystal C^+ axis, the pumping direction, and the cavity axis. The losses are biased by the scattering in the crystal, the reflectivity of the mirrors, and the Fresnel reflection at the crystal facets, but can be modified by means of apertures. The detuning can be modified by fine adjustment of the cavity length, as described below. Finally, using a near self-imaging resonator [16] the effective length of the resonator can take any desired value (in magnitude and sign, including zero), allowing the control of the diffraction.

A scheme of the setup is shown in Fig. 1. Pump beams (P1 and P2), from a single frequency Ar^+ laser at 514.5 nm and typical intensities of 100 mW/cm^2 , illuminate the BaTiO_3 crystal ($5 \times 5 \times 5 \text{ mm}^3$). From the operational point of view the system is composed of the nearly self-imaging active resonator (similar to those used in Refs. [12,17]), the stabilization resonator [18], and the observation and measurement systems.

The active Fabry-Perot resonator is formed by mirrors M1 and PM4, both of 95 % reflectivity. The C^+ axis of the crystal is oriented to maximize the coupling efficiency of the pumps inside the resonator, keeping it in the horizontal plane.

The pump beams are horizontally polarized (in the plane of the drawing), and are extraordinarily polarized in the crystal. As a result, the generated field will also be horizontally polarized and will pass through the polarizing beam splitters PBS1 and PBS2. The high reflectivity piezomirror PM2 bends the path to complete the resonator. Self-imaging condition is achieved by means of two telescopes (lenses L1-L2 and L3-L4), which image mirrors M1 and PM4 onto (or very closely to) the crystal location. The effective cavity length can be varied by coarse axial displacement of piezomirror PM4. This telescopic arrangement also provides easy access to the far-field (Fourier) pattern in the intermediate focal planes FP1 and FP2. In our experiments, in order to permit transverse modes, the mirror PM4 is shifted 4.50 cm from the self-imaging position. The finesse of the active resonator is really small: The transmission T of the resonator was measured as a function of the driving voltage applied to PM2, and the data were fitted to an Airy function, $T = 1/[1 + F \sin^2(\delta/2)]$, with the result $F = 0.23 \pm 0.04$ (see Fig. 2).

The other polarization (perpendicular to the plane of the drawing) is used for optical length stabilization purposes, feeding a small amplitude signal (REF) through mirror M1.

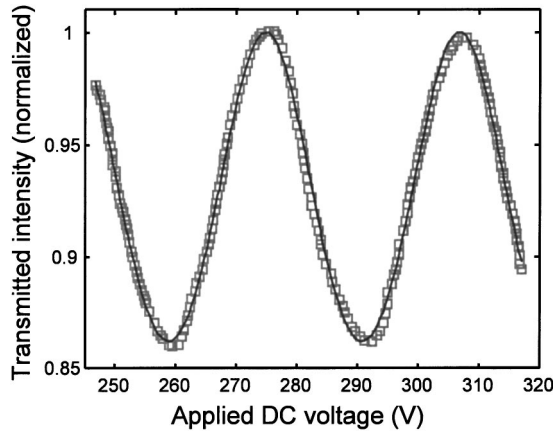


FIG. 2. Transmission properties of the active resonator. Squares: measured transmitted intensity as a function of the dc voltage applied to PM2. Continuous line: the best fitting Airy function.

Light is reflected on both polarizing beam splitters (PBS1 and PBS2), and the high reflectivity piezomirror PM3 completes the control resonator. The finesse of this resonator (over 10) is appropriate for fine adjustment of the cavity length. Piezomirror PM3 is driven by a periodic voltage and the variation of the resonator transmission, measured by photodetector PD2, is then used in a feedback loop to drive mirror PM4 and correct the resonator length variations. Finally, the piezomirror PM2 allows fine variation of the active cavity length without interfering with the stabilization. It can be modulated as well with a periodic voltage in order to use the resonances of the active cavity (including the crystal) detected in PD1 to measure the drift of the active cavity with respect to the control one. The subsystem formed by PBS1, PBS2, PM3, PM2, and the crystal is held on a rigid and stable Invar plate which is also shielded from air currents so that the optical path difference between active and stabilization resonators is kept constant except for small drifts. The stability of the system is very good, although in rare occasions we found drifts in the cavity frequency on the order of 0.2 MHz/min. In any case we checked that our measurements were not affected by this drift, as we will discuss.

In order to simplify the study, the transverse dimensions are reduced to one. This simplification permits the description with a lower number of parameters and avoids curvature effects that may mask the results. The system is made one dimensional by means of slits S2 and S3, 100 μm width, located at both Fourier planes. The length of the slits in the Fourier planes is adjusted in order to avoid multiconical emission corresponding to different longitudinal modes. The insertion of the slits should produce a one-dimensional field in the crystal plane, without variation in the direction perpendicular to the slit. Nevertheless, owing to crystal inhomogeneities, the effective cavity length may vary for different transverse areas of the crystal. Additional broader slits (S1 and S2) of 400 μm are then located in the primary mirrors that select a sufficiently uniform portion of the active medium.

The system is complemented with the image acquisition subsystem (at the left of the figure). Lenses L5–L7 are used

to image the crystal exit face and the Fourier plane FP2 onto charge-coupled device cameras CCD1 and CCD2.

III. EXPERIMENTAL PROCEDURE

Once the system is stabilized, we are able to change detuning by means of a dc voltage applied to the piezomirror PM2 which modifies the optical length of the active resonator. As the cavity length is very large as compared to the tiny displacements of PM2 (of the order of the light wavelength), which are admittedly linear on the dc voltage variations, the cavity eigenfrequencies also depend linearly on this voltage.

The voltage was changed in 1 V steps in order to study the behavior of the spatial patterns with detuning. Recording time was about 1 min to avoid the possible detuning shift due to the drift of the active resonator. An example of the so-obtained patterns is shown in Fig. 3 corresponding to decreasing voltage values (decreasing cavity frequencies) from (a) to (k). A homogeneous state (a), a domain wall (b), and periodic stripes (g)–(j) are shown, which are connected by a series of nonperiodic striped patterns (c)–(f). All these patterns are steady, except the transient competition between rolls of high spatial frequency and the homogeneous state shown in (k). Further decreasing voltage from (k) the system falls onto a homogeneous state and the above sequence is repeated. We note that, when two-dimensional patterns are allowed, phase domains (closed domain walls) are generic for this system at positive detunings [19].

In order to test law (1) both the transverse wave-number k_{\perp} and the cavity detuning Ω must be measured. The first is trivially determined by measuring the spatial period of rolls, Λ , from the digitized images, from which $k_{\perp} = 2\pi/\Lambda$. Detuning measurement is more involved. In principle Ω can be measured by determining the cavity free spectral range (FSR) in terms of the applied dc voltage (in our setup one FSR was completed after an increase of 33 ± 1 V). However, we need to know further at which voltage values zero detuning (exact resonance) is achieved. This last part is not easy to assess at all and we proceeded as follows. Two consecutive series of rolls, corresponding to adjacent longitudinal modes, were scanned. Figure 4 shows the relation between the squared wave number of rolls and voltage for the two consecutive series. Data corresponding to nonperiodic patterns are not depicted. A linear relation between k_{\perp}^2 and the applied voltage V is apparent. The horizontal distance between the two straight lines is the FSR by definition, and the intersection of these lines with the axis $k_{\perp}^2 = 0$ defines, according to Eq. (1), the voltages at which the cavity detuning $\Omega = 0$. Both series were fitted to a linear relation

$$k_{\perp}^2 = -\alpha \Delta V,$$

$$\Delta V = V - V_0, \quad (2)$$

with the result $\alpha_1 = (5.30 \pm 0.09) \times 10^{-5} \mu\text{m}^{-2} \text{V}^{-1}$ for the left one and $\alpha_2 = (5.31 \pm 0.07) \times 10^{-5} \mu\text{m}^{-2} \text{V}^{-1}$ for the right one. The fact that both slopes coincide indicates that the drift of the cavity resonances is not important in these measurements as well as allows us to determine the cavity FSR in terms of

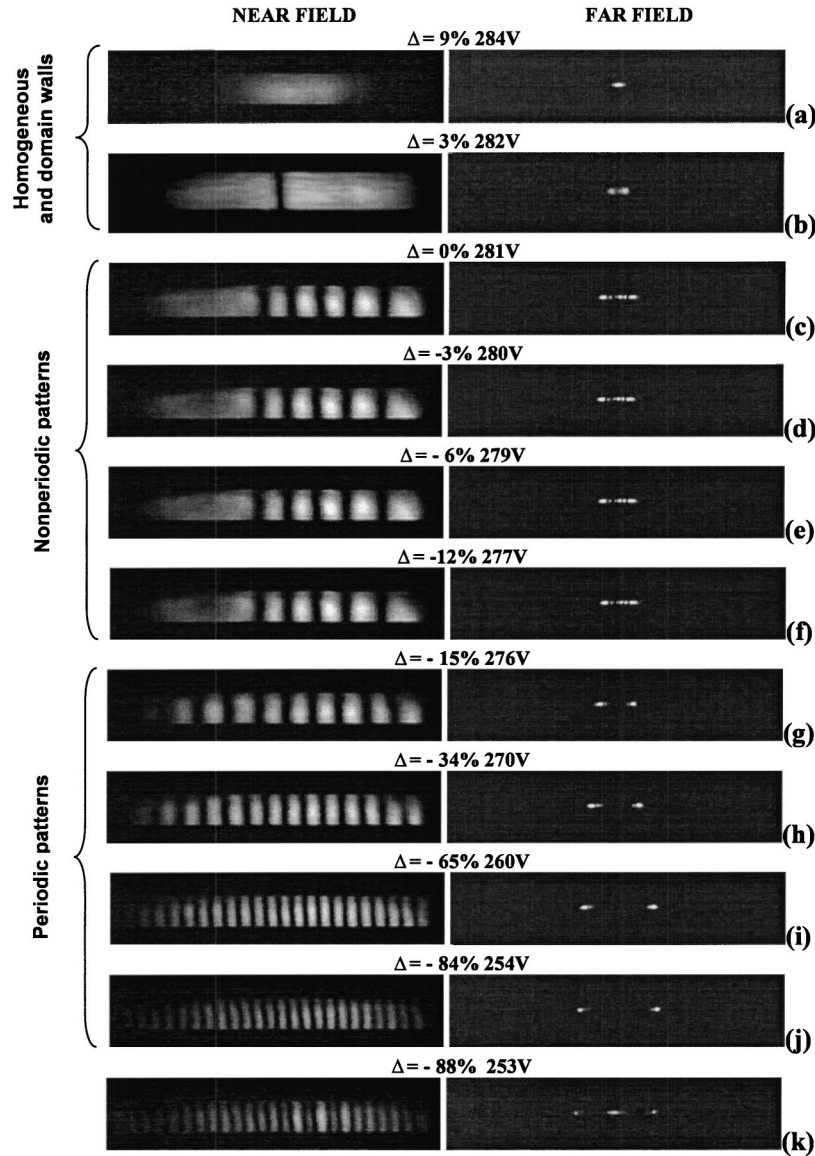


FIG. 3. Experimental recordings of the near (left) and far (right) fields under different detunings Δ measured in percentage of the free spectral range. Also the voltage applied on the piezomirror PM2 is indicated.

the applied voltage, which evaluates $\Delta V_{\text{FSR}} = 31.9 \pm 0.3$ V. Note that this value compares well with the direct measurement of the cavity FSR, 33 ± 1 V, based on the scanning of the cold resonator through piezomirror PM2. We would like to note that the indirect method is more precise than the direct one, especially because of the lack of precision in the measurement on the screen of the oscilloscope, due to the low finesse (smaller than 1) of the active resonator. Once the FSR is precisely known in terms of applied voltage, we can relate it with its actual value. In the experiment the optical length of the cavity was $L = 1.25 \pm 0.01$ m, hence the FSR is equal to $c/2L = 120 \pm 1$ MHz.

Finally we note two further observations from Fig. 4. On the one hand the highest wave numbers for both series do not fit to the straight lines as good as the others because of the limitation induced by the diaphragm. On the other hand, the plot is not reaching to zero wave number because the periodicity for these cases does not exist as commented.

IV. WAVE-NUMBER SELECTION VERSUS CAVITY DETUNING

From the value of FSR obtained as 120 ± 1 MHz, the fact that a voltage increase of $\Delta V_{\text{FSR}} = 31.9 \pm 0.3$ V is needed to scan one FSR, and the assumed linear relation between voltage increase and detuning, we arrive at the correspondence $\Omega = f\Delta V$, with $f = 2\pi\text{FSR}/\Delta V_{\text{FSR}} = (23.6 \pm 0.4) \times 10^6 \text{ s}^{-1} \text{ V}^{-1}$ (the factor 2π is included as Ω is defined in terms of angular frequencies). Hence relation (2) can be written as

$$k_{\perp}^2 = -\Omega/a_{\text{expt}}, \quad (3)$$

where

$$a_{\text{expt}} = f/\alpha = 0.445 \pm 0.015 \text{ m}^2 \text{ s}^{-1}, \quad (4)$$

and $\alpha = (5.30 \pm 0.09) \times 10^{-5} \text{ } \mu\text{m}^{-2} \text{ V}^{-1}$ has been used. Hence law (1) is proven.

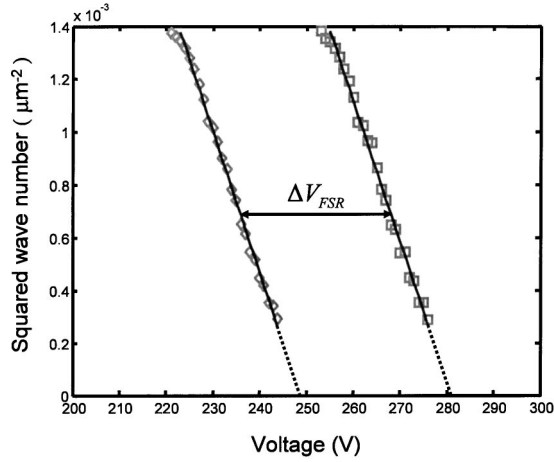


FIG. 4. Dependence of the spatial frequency of rolls on the voltage applied on the piezomirror PM2, corresponding to two consecutive longitudinal modes. Diamonds and squares correspond to experimental data. Straight lines correspond to fits of the data to Eq. (2).

We now study how Eq. (4) compares with the theoretical prediction based on the assumption that wave-number selection is governed by the resonance of tilted waves in the resonator. For that we note, referring to Fig. 5, that the phase accumulated by a tilted wave of optical frequency ω and transverse wave-number k_{\perp} along a resonator round trip can be written, in the paraxial approximation, as

$$\phi(k_{\perp}) = \phi(0) - \frac{cl}{\omega} k_{\perp}^2, \quad (5)$$

where $l = (-l_1 + l_2 + d/n)$ is the effective length of the cavity (the resonator is exactly self-imaging when $l=0$), c is the speed of light in vacuum, n is the refractive index of the crystal, and

$$\phi(0) = 2\omega L/c, \quad (6)$$

where $L = (L_1 + L_2 - l_1 + l_2 + nd)$ is the optical length of the resonator. Note in the previous expressions that l_1 and l_2 are oriented distances (see Fig. 5 caption). The frequencies of the cavity longitudinal modes, ω_c , are defined by the condition $\phi(0) = 2m\pi$, m being integer, which yields $\omega_{c,m} = m\pi c/L$. If we express the wave frequency ω as $\omega = \omega_c - \Omega$, relation (5) predicts that a transverse wave number will be

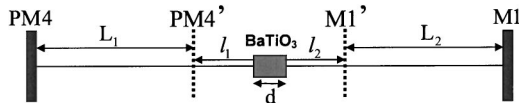


FIG. 5. Scheme of the nearly self-imaging resonator. Only the main elements are depicted. PM4' and M1' are the image planes of PM4 and M1 (see Fig. 1) through the corresponding telescopes and beam splitters. The distances l_1 and l_2 are oriented, being positive (negative) if they point to the right (left). The length of the crystal is denoted by d . The optical path of tilted waves only differs from that of on-axis waves in their propagation between PM4' and M1'.

resonant, i.e., $\phi(k_{\perp}) = 2p\pi$, p being integer, if it verifies the following relation:

$$k_{\perp}^2 = (q\pi c/L - \Omega)/a, \quad (7)$$

where $q = p - m$ is an integer and

$$a = \frac{c^2 l}{2\omega L}. \quad (8)$$

We observe that if we restrict to the longitudinal mode whose frequency is closest to that of the wave (then $q=0$), which is the single longitudinal mode approximation, relation (7) becomes law (1). Values of q different from zero account for the multiconical emission observed in this type of experiments which in our case are ruled out by the insertion of slits in the Fourier planes. Using the experimental values $l = 4.50 \pm 0.01$ cm, $L = 1.25 \pm 0.01$ m, and $\omega = 3.659 \times 10^{15}$ s⁻¹ ($\lambda = 514.8$ nm), we obtain

$$a_{\text{theory}} = 0.442 \pm 0.005 \text{ m}^2 \text{ s}^{-1}, \quad (9)$$

which coincides, within the error interval, with the experimentally determined diffraction coefficient (4).

It is to be pointed out that wave-number selection has been theoretically explained in terms of the modal structure of the cold cavity (including only linear contributions). This means that nonlinear phase shifts possibly given by the photorefractive effect or, in general, nonlinear dispersion (due, e.g., to the nonlinear resonance effect [20]) are apparently absent in our experiment.

We note from Eq. (8) that in our resonator the diffraction coefficient can be controlled by means of the offset l , and can take both positive, negative and null values, as commented.

It is instructive to think of Eq. (7) in terms of a graphical construction as follows. In the used paraxial approximation, the longitudinal component k_{\parallel} of the wave vector can be written as $k_{\parallel} = \omega/c - k_{\perp}^2 c/2\omega$. Hence, from Eqs. (7) and (8), we obtain that a wave of longitudinal wave number k_{\parallel} will be in resonance with the cavity if it verifies

$$k_{\parallel} = \omega/c + L\Omega/cl - q\delta k_{\text{eff}}, \quad (10)$$

with $\delta k_{\text{eff}} = \pi/l$. Thus, the resonance condition for a tilted wave can be seen as determined by the intersection of a circumference of radius $k = \omega/c$ with a comb of vertical lines separated by the fundamental wave number of the effective cavity, δk_{eff} , whose location depends on the cavity detuning Ω . This construction will be used in the following section for understanding the behavior of the system.

V. PHYSICAL ORIGIN OF THE NONPERIODIC PATTERNS

Figure 6 corresponds to one of the series shown in Fig. 4, but now the horizontal axis is detuning measured in units of % FSR (let us call it Δ). For negative detuning Δ (ranging from -90% FSR to 0% FSR) stripes are observed, being periodic rolls in region A and nonperiodic patterns in region B [like in Figs. 3(c)–3(f)]. At zero and positive Δ we observe

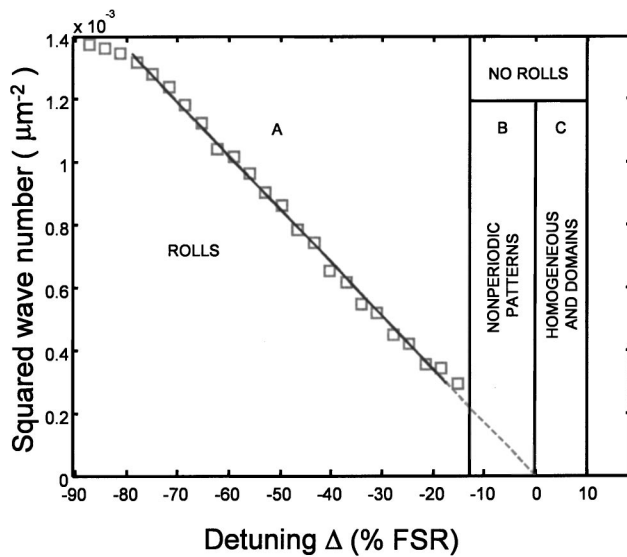


FIG. 6. Relation between the squared wave number of rolls and detuning for one free spectral range. Regions A, B, and C correspond to different emission patterns, according to the labels.

either a homogeneous field or domain walls, as expected. We finally note that for large and negative detuning (around $\Delta = -90\%$ FSR) axial emission competes with tilted waves of high spatial frequency corresponding to the next longitudinal mode. Owing to nonlinear competition sometimes the central spot at the far field takes all the energy but sometimes rolls win.

Especially interesting is region B. Figure 7 shows a series of patterns obtained at the two sides, close to the line that separates regions A and B in Fig. 6, for three consecutive longitudinal modes. We see that these nonperiodic patterns are robust structures of the system in the region of small, negative detuning. We note that the transition from periodic (roll) to nonperiodic patterns occurs at the same detuning value, independently of the direction of the scan, i.e., both by increasing or decreasing detuning. Clearly the transient stage is different in both cases: if detuning is increased from region A in Fig. 6 what is observed is the annihilation of some of the already present stripes, whereas by decreasing detuning from region C in Fig. 6 creation of isolated stripes is observed. In any case the final state is a collection of stripes separated by apparently random distances. In the far field what is observed (see Fig. 7) is that these nonperiodic pat-

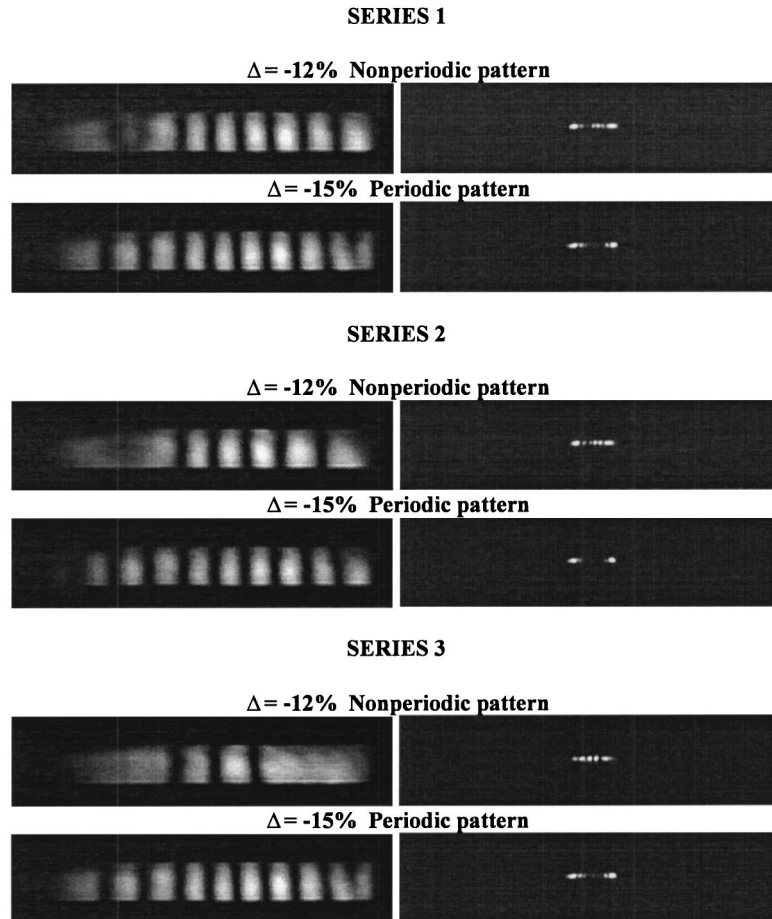


FIG. 7. Experimental recordings of both the near (left) and far (right) field for three different longitudinal modes corresponding to the transition between regions A and B in Fig. 6. By decreasing detuning the periodicity of stripes is broken in the near field, which manifests in the far field through the appearance of additional spots between the two which correspond to the periodic roll pattern.

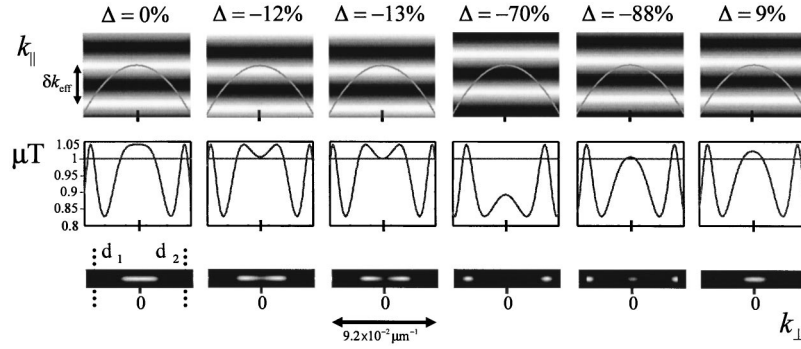


FIG. 8. Interpretation of the spatial frequency selection mechanism. Top row: density plot of the Airy function of the active resonator on the plane $k_{||}$ vs k_{\perp} ; the parabolic-like curve represents all possible wave vectors of the light. Middle row: assumed linear gain as a function of k_{\perp} ; the horizontal line denotes the oscillation threshold. Bottom row: far-field intensity as predicted by Eq. (14); d_1 and d_2 denote the borders of the slits located at the Fourier plane. In all figures the horizontal axis corresponds to k_{\perp} and its size is indicated. Each column corresponds to a given cavity detuning marked on the top. For details, see Sec. V.

terns contain a large number of small transverse wave numbers. We ask why.

An explanation of this effect can be given by considering the graphical construction already introduced at the end of the preceding section, in combination with the fact that the cavity resonances are not sharp (recall that the F factor of its associated Airy function equals 0.23). The upper row in Fig. 8 shows a scheme of the graphical construction given by Eq. (10) for six detuning values scanning a complete free spectral range. Each figure displays a density plot of the Airy function of the cavity (hence it shows its resonance structure) which solely depends on the longitudinal wave number, together with a circumference of radius $k = \omega/c$ representing the light wave number (its appearance is parabolic as the horizontal axis, which corresponds to the transverse wave number, has been squeezed). According to Eq. (10) the intersections between that circumference and the cavity resonances should give the selected transverse wave number. However, due to the low finesse of the cavity that selection mechanism is quite tolerant and, close to resonance, it is feasible that a broad band of small transverse wave numbers fits simultaneously the tilted wave conditions (7) and (10). But we can try to be more predictive if we adopt, without trying to be rigorous, the following simplest model: Assume that the observed emitted intensity at a given transverse wave number, $I(k_{\perp})$, follows the simple law

$$\frac{g(k_{\perp})}{1 + I(k_{\perp})/I_s} = \gamma, \quad (11)$$

where $g(k_{\perp})$ represents the linear gain for a given tilt, γ represents losses (assumed equal for all waves), and I_s is a saturation intensity. We are thus assuming that the amplification mechanism is that of the simplest form of gain saturation (note that we are ignoring the phase sensitive nature of the four-wave mixing process). Assume further that the linear gain equals the product of a pump parameter g_0 (which should be related with the ratio between pump beam intensities [21]) and the Airy function of the resonator $T(k_{\perp})$, i.e.,

$$g(k_{\perp}) = g_0 T(k_{\perp}), \quad (12)$$

where [22]

$$T(k_{\perp}) = \frac{1}{1 + F \sin^2 \frac{\phi(k_{\perp})}{2}}, \quad (13)$$

$F = 0.23 \pm 0.04$ in our experiment and $\phi(k_{\perp})$ is the phase accumulated by a tilted wave of optical frequency ω and transverse wave number k_{\perp} along a resonator round trip and is given by Eqs. (5) and (6). It can be written in terms of the cavity detuning Ω as $\phi(k_{\perp}) = -2\Omega L/c - k_{\perp}^2 cl/\omega$, modulo 2π . The reason to include T in the gain is purely phenomenological: we are adopting a simple picture in which those waves that are closer to the longitudinal resonances experience more net gain than those which are off-resonant, and we assume that this is just proportional to the transmission properties of the resonator (we could consider, alternatively, that T controls the cavity losses and hence γ should be inversely proportional to T ; we prefer however to use the proposed picture as, in fact, cavity losses, understood as the parameter giving the loss of photons per unit time, are the same for all tilts, if we ignore diffraction losses). Use of Eq. (12) into Eq. (11) yields

$$I(k_{\perp})/I_s = \mu T(k_{\perp}) - 1, \quad (14)$$

where $\mu = g_0/\gamma$ represents the linear gain to loss ratio for waves exactly on resonance with the cavity. By fitting the Fourier spectral intensities of the different observed patterns to Eq. (14) we obtained that $\mu = 1.04$ is able to reproduce the measured spectra for all cavity detunings (note that μ is the single fitting parameter: I_s is just a proportionality factor). The middle row in Fig. 8 displays the function $\mu T(k_{\perp})$ as a function of the transverse wave number, and the bottom row displays the associated density plots of the predicted far-field pattern according to Eq. (14). Note that the predicted far fields compare well with our experimental observations (see Fig. 3). Especially note, around zero detuning, how a set of tilted waves (also the on-axis one)

can be oscillating. Therefore we expect, and observe (Fig. 3), dissipative structures, but they are not periodic as the wave-number selection mechanism given by the cavity does not work in a clean way here. Clearly the above is a linear reasoning but we have checked experimentally that these nonperiodic patterns are not a transient stage: some spots can change their intensity as well as their shape, but there is always a broad Fourier spectrum (of low spatial frequency content). Under these conditions, we can see stripes in movement in the near field.

All the previous discussions lead us to the idea that each tilted wave has its own amplification, almost independently of the presence of other waves [note that the gain in Eq. (11) does not consider cross saturation]. This low nonlinearity can be reasonably understood as the obtained value for $\mu=1.04$ is only 4% over threshold [according to Eq. (14), $\mu=1$ corresponds to the threshold for oscillation].

VI. CONCLUSIONS

Pattern formation in a large Fresnel number (nearly self-imaging), Fabry-Perot, BaTiO₃ photorefractive oscillator in a degenerate four-wave mixing configuration has been investigated in relation with the transverse wave-number selection problem. The system was made transversely one dimensional in order to avoid curvature effects. The main goal of the

work was to provide evidence of the transverse wave-number selection mechanisms existing in cavity nonlinear optics. A careful stabilization of the cavity allowed a good control of the cavity detuning which could be measured. The obtained results show repetitivity and hence provide a solid base for its study. The main conclusion is that transverse wave-number selection is mainly brought about by the cavity geometry. This is true for negative detunings where the experimentally obtained and theoretically computed diffraction coefficients fully agree. Even more surprising, we find that nonperiodic patterns observed at small negative detunings can be explained on the same basis as well, when the finite linewidth of the cavity is taken into account. Nonlinear effects, while present, do not seem to affect strongly the selection mechanism in our experiment.

ACKNOWLEDGMENTS

Financial support from the Spanish Ministerio de Ciencia y Tecnología and the European FEDER (Project Nos. BFM2002-04369-C04-01 and BFM2001-3004), and from the Agencia Valenciana de Ciencia i Tecnología (AVCT Project No. GRUPOS03/117) is acknowledged. A.E.-M. acknowledges a grant from the Spanish Ministerio de Educación, Cultura y Deporte. V.B.T. was partially supported by the Generalitat Valenciana (Valencian Government, Grant No. CTESIN/2003/006).

-
- [1] P. Manneville, *Dissipative Structures and Weak Turbulence* (Academic Press, New York, 1990).
 - [2] M. C. Cross and P. C. Hohenberg, *Rev. Mod. Phys.* **65**, 851 (1993).
 - [3] D. Walgraef, *Spatio-Temporal Pattern Formation* (Springer, Berlin 1996).
 - [4] P. Mandel, *Theoretical Problems in Cavity Nonlinear Optics* (Cambridge University Press, Cambridge, 1997).
 - [5] L. A. Lugiato, M. Brambilla, and A. Gatti, *Optical Pattern Formation*, special issue of *Adv. At., Mol., Opt. Phys.* **40**, 229 (1999).
 - [6] K. Staliunas and V. J. Sánchez-Morcillo, *Transverse Patterns in Nonlinear Optical Resonators* (Springer, Berlin, 2002).
 - [7] P. K. Jacobsen, J. V. Moloney, A. C. Newell, and R. Indik, *Phys. Rev. A* **45**, 8129 (1992).
 - [8] W. J. Firth and A. J. Scroggie, *Europhys. Lett.* **26**, 521 (1994).
 - [9] T. P. Dawling, M. O. Scully, and F. De Martini, *Opt. Commun.* **82**, 415 (1991).
 - [10] K. Staliunas, G. Sleky, and C. O. Weiss, *Phys. Rev. Lett.* **79**, 2658 (1997).
 - [11] A. V. Mamaev and M. Saffman, *Opt. Commun.* **128**, 281 (1996).
 - [12] V. B. Taranenko, K. Staliunas, and C. O. Weiss, *Phys. Rev. Lett.* **81**, 2236 (1998).
 - [13] S. P. Hegarty, G. Huyet, J. G. McInerney, and K. D. Choquette, *Phys. Rev. Lett.* **82**, 1434 (1999); S. P. Hegarty, G. Huyet, P. Porta, J. G. McInerney, K. D. Choquette, K. M. Geib, and H. Q. Hou, *J. Opt. Soc. Am. B* **16**, 2060 (1999).
 - [14] T. Ackemann, S. Barland, J. R. Tredicce, M. Cara, S. Balle, R. Jäger, M. Grabherr, M. Miller, and K. J. Ebeling, *Opt. Lett.* **25**, 814 (2000).
 - [15] U. Bortolozzo, P. Villoresi, and P. L. Ramazza, *Phys. Rev. Lett.* **87**, 274102 (2001).
 - [16] J. A. Arnaud, *Appl. Opt.* **8**, 189 (1969).
 - [17] K. Staliunas, V. B. Taranenko, G. Sleky, R. Viselga, and C. O. Weiss, *Phys. Rev. A* **57**, 599 (1998).
 - [18] M. Vaupel and C. O. Weiss, *Phys. Rev. A* **51**, 4078 (1995).
 - [19] Ye. Larionova, U. Peschel, A. Esteban-Martín, J. García-Monreal, and C. O. Weiss, *Phys. Rev. A* **69**, 033803 (2004).
 - [20] G. J. de Valcárcel, K. Staliunas, V. J. Sánchez-Morcillo, and E. Roldán, *Phys. Rev. A* **54**, 1609 (1996).
 - [21] P. Yeh, *Introduction to Photorefractive Nonlinear Optics* (Wiley, New York, 1993).
 - [22] M. Born and W. Wolf, *Principles of Optics* (Cambridge University Press, Cambridge, 1999), pp. 363 ff.